A New Powerful Source for Coherent VUV Radiation: Demonstration of Exponential Growth and Saturation at the TTF Free-Electron Laser

V. Ayvazyan,[4] N. Baboi,[7] I. Bohnet,[5] R. Brinkmann,[4] M. Castellano,[8] P. Castro,[4] L. Catani,[10] S. Choroba,[4] A. Cianchi,[10] M. Dohlus,[4] H.T. Edwards,[6] B. Faatz,[4] A.A. Fateev,[13] J. Feldhaus,[4] K. Flöttmann,[4] A. Gamp,[4] T. Garvey,[14] H. Genz,[3] Ch. Gerth,[4] V. Gretchko,[11] B.Grigoryan,[19] U. Hahn,[4] C. Hessler,[3] K. Honkavaara,[4] M. Hüning,[17] R. Ischebeck,[17] M. Jablonka,[1] T. Kamps,[5] M. Körfer,[4] M. Krassilnikov,[2] J. Krzywinski,[12] M. Liepe,[7] A. Liero,[17] T. Limberg,[4] H. Loos,[3] M. Luong,[1] C. Magne,[1] J. Menzel,[17] P. Michelato,[9] M. Minty,[4] U.-C. Müller,[4] D. Nölle,[4] A. Novokhatski,[2] C. Pagani,[9] F. Peters,[4] J. Pflüger,[4] P. Piot,[4] L. Plucinski,[7] K. Rehlich,[4] I. Reyzl,[4] A. Richter,[3] J. Rossbach,[4,20] E.L. Saldin,[4] W. Sandner,[15] H. Schlarb,[7] G. Schmidt,[4] P. Schmüser,[7] J.R. Schneider,[4] E.A. Schneidmiller,[4] H.-J. Schreiber,[5] S. Schreiber,[4] D. Sertore,[9] S. Setzer,[2] S. Simrock,[4] R. Sobierajski,[4,18] B. Sonntag,[7] B. Steeg,[4] F. Stephan,[5] K.P. Sytchev,[13] K. Tiedtke,[4] M. Tonutti,[17] R. Treusch,[4] D. Trines,[4] D. Türke,[17] V. Verzilov,[8] R. Wanzenberg,[4] T. Weiland,[2] H. Weise,[4] M. Wendt,[4] T. Wilhein,[16] I. Will,[15] S. Wolff,[4] K. Wittenburg,[4] M.V. Yurkov,[13] and K. Zapfe[4]

[1] *CEA Saclay, 91191 Gif s/Yvette, France*
[2] *Darmstadt University of Technology, FB18 - Fachgebiet TEMF, Schlossgartenstr. 8, 64289 Darmstadt, Germany*
[3] *Darmstadt University of Technology, Institut für Kernphysik, Schlossgartenstr. 9, 64289 Darmstadt, Germany*
[4] *Deutsches Elektronen-Synchrotron DESY, Notkestrasse 85, 22603 Hamburg, Germany*
[5] *Deutsches Elektronen-Synchrotron DESY, Platanenallee 6, 15738 Zeuthen, Germany*
[6] *Fermi National Accelerator Laboratory, MS 306, P.O. Box 500, Batavia, IL 60510 USA*
[7] *Hamburg University, Inst. f. Experimentalphysik, Notkestrasse 85, 20603 Hamburg, Germany*
[8] *INFN-LNF, via E. Fermi 40, 00044 Frascati, Italy*
[9] *INFN Milano - LASA, via Fratelli Cervi 201, 20090 Segrate (MI), Italy*
[10] *INFN-Roma2, via della Ricerca Scientifica 1, 00100 Roma, Italy*
[11] *Institute for Nuclear Research of RAS, 117312 Moscow, 60th October Anniversary prospect 7A, Russia*
[12] *Institute of Physics, Polish Academy of Sciences, al. Lotnikow, 32/46, 02-668 Warsaw, Poland*
[13] *Joint Institute for Nuclear Research, 141980 Dubna, Moscow Region, Russia*
[14] *Laboratoire de l'Accélérateur Linéaire, IN2P3-CNRS, Université de Paris-Sud, B.P. 34, F-91898 Orsay, France*
[15] *Max-Born-Institute, Max-Born-Str. 2a, 12489 Berlin, Germany*
[16] *Rhein-Ahr-Campus Remagen, Südallee 2, 53424 Remagen, Germany*
[17] *RWTH Aachen-Physikzentrum, Phys. Inst. IIIa, Sommerfeldstr. 26-28, 52056 Aachen, Germany*
[18] *Warsaw University of Technology, Institute of Physics, Poland*
[19] *Yerevan Physics Institute, 2 Alikhanyan Brothers str., 375036 Yerevan, Armenia*
[20] *corresponding author; e-mail: joerg.rossbach@desy.de*

We present experimental evidence that the free-electron laser at the TESLA Test Facility has reached the maximum power gain of 10^7 in the vacuum ultraviolet (VUV) region at wavelengths between 80 and 120 nm. At saturation the FEL emits short pulses with GW peak power and a high degree of transverse coherence. The radiation pulse length can be adjusted between 30 fs and 100 fs. Radiation spectra and fluctuation properties agree with the theory of high gain, single-pass free-electron lasers starting from shot noise.

PACS numbers: 41.60.Cr,29.17.+w,29.27.-a.Fh,41.75.Lx,29.25.Bx,52.75.Va

INTRODUCTION

Over the past 30 years, the synchrotron radiation has been developed into a most powerful research tool with applications in many different fields of science ranging from physics, chemistry and biology to materials sciences, geophysics and medical diagnostics. Rapid progress was driven by improvements in the technology of electron storage rings and of periodic arrays of magnets called undulators thus providing increasingly brilliant sources of synchrotron radiation. The radiation generated in these devices is based on spontaneous radiation of many electrons uncorrelated in space and time. As a consequence, the radiation power scales linearly with the number N_e of electrons, and the radiation exhibits only limited coherence in space and time.

In order to increase the power and the coherence of the radiation one has to force the electrons to emit coherently by compressing them into a length small compared to the wavelength of the radiation. Passing such a "point-like" bunch of relativistic energy electrons through an undulator would cause a dramatic boost of the radiation power $P_{rad} \propto {N_e}^2$ with N_e the number of electrons in the bunch. Such a tight compression of an entire bunch is not possible for wavelengths in the nanometer regime. However, if one succeeds to arrange a large number of

"point-like" bunchlets longitudinally into a periodic array, with the periodicity given by the wavelength of radiation, one obtains indeed coherent radiation of these bunchlets with the additional advantage of compressing all the radiation into a narrow forward cone. The principle of the Free-Electron Laser (FEL), first demonstrated with a relativistic electron beam by Madey and his colleagues [1, 2], is based on this idea.

In an FEL, a bunch of electrons with length much longer than the desired wavelength is effectively "cut" into slices with the periodicity of the radiation wavelength by a resonant process taking place in the combined presence of the periodic transverse magnetic field of an undulator and the electromagnetic radiation generated in this same magnet. The wavelength λ_{ph} of the first harmonic of the FEL radiation is related to the period length λ_u of a planar undulator by

$$\lambda_{ph} = \frac{\lambda_u}{2\gamma^2}\left(1 + \frac{K^2}{2}\right) \qquad (1)$$

where $\gamma = E/(m_e c^2)$ is the relativistic factor of the electrons, $K = eB_u\lambda_u/2\pi m_e c$ is the 'undulator parameter' with B_u being the peak magnetic field in the undulator, m_e the electron rest mass and c the speed of light. Equation 1 exhibits two main advantages of the free-electron laser: the free tunability of the wavelength by changing the electron energy or the magnetic field, and the possibility of achieving very short photon wavelengths by using ultra-relativistic electrons.

For most FELs presently in operation [3], the electron beam quality and the undulator length result in a gain in radiation power of up to a few 100% per undulator passage. Thus an optical cavity resonator and a synchronized multi-bunch electron beam have to be used in order to build up high radiation brightness upon several passages of an electron beam through the undulator. At very short wavelengths, normal-incidence mirrors of high reflectivity are unavailable thus demanding that the maximum gain be reached within a single passage through the undulator. To this end, the generation of an electron beam with extremely small spatial dimensions, high peak current and small energy spread, and a high-precision undulator of sufficient length are essential.

Provided the input radiation present in the first part of the undulator overlaps the electron beam, the electromagnetic radiation interacts with the electron bunch leading to a steadily growing density modulation (microbunching) which enhances the power and coherence of radiation. In this "high gain mode" [4–6], the radiation power $P(z)$ grows exponentially with the distance z along the undulator (see Fig. 1)

$$P(z) = P_0 \cdot A \cdot exp(z/L_g) \qquad (2)$$

where L_g is the power gain length and P_0 the effective input power (see below). The input coupling factor [5, 6]

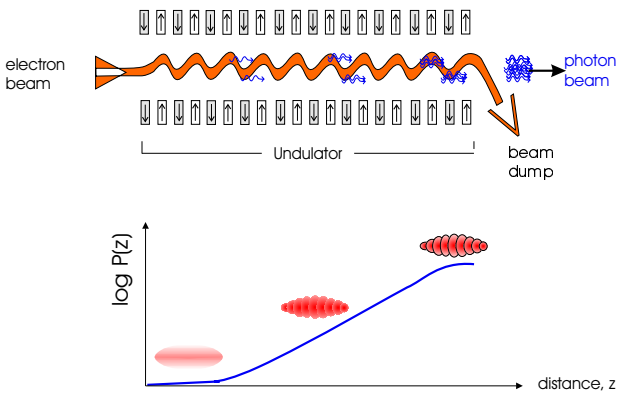

FIG. 1: Schematic diagram of a Single-Pass Free Electron laser (FEL) operating in the Self-Amplified-Spontaneous - Emission (SASE) mode (top) and the bunch charge density modulation, developing in parallel to the radiation power (bottom). Note that in reality the frequency of the density modulation within the bunch (i.e. the number of "slices") is much larger.

A is equal to 1/9 in one-dimensional FEL theory with an ideal electron beam. At the end of this process, when the electron bunch is completely modulated, i.e. "cut into slices" as explained above, laser saturation sets in and no further power gain is possible.

For very short wavelengths below the visible, there exists no laser which is tunable over a wide range and could provide the input power P_0. Instead, the spontaneous undulator radiation from the first part of the undulator is used as an input signal to the amplification process. Since a decade, FELs based on this Self-Amplified-Spontaneous-Emission (SASE) principle [7, 8] are considered the most attractive candidates for extremely brilliant, coherent light sources with wavelengths down to the Ångström regime [9–12]. Compared to state-of-the-art synchrotron radiation sources, one expects full transverse coherence, larger average brilliance and, in particular, up to eight or more orders of magnitude larger peak brilliance (see Figure 2) at pulse lengths of about 100 fs FWHM. In terms of peak power, coherence and tunability, FELs are also superior to other lasers or frequency conversion schemes aiming at VUV and X-ray wavelengths (see for example Ref. [13]).

The present paper reports on the first demonstration of such spectacular performance of a SASE FEL for wavelengths around 100 nm, i.e. in a wavelength range not directly accessible by conventional lasers. In the past three years, high SASE gain and saturation have been achieved at longer wavelengths [14, 15] in proof-of-principle experiments. The present vacuum-ultraviolet (VUV) FEL is, in addition to proving the principle, a most attractive radiation source for many scientific users. First exciting results on the interaction of the high power FEL photon beam with solids and clusters have already been ob-

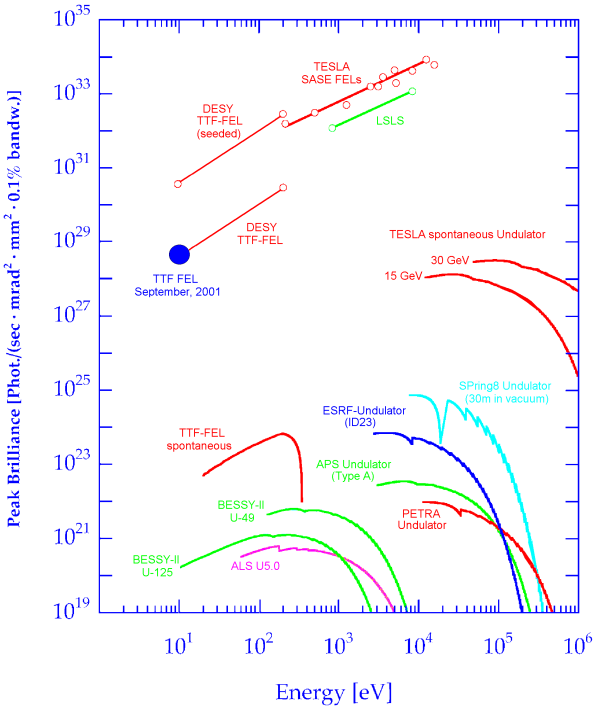

FIG. 2: Expected spectral peak brilliance of proposed SASE FELs as well as the spontaneous emission from these devices in comparison with state-of-the-art synchrotron radiation sources. The large dot marks the experimental result from the TTF FEL.

tained.

EXPERIMENTAL SET-UP

The experimental results presented in this paper have been achieved at the TESLA Test Facility (TTF) Free-Electron Laser [16] at the Deutsches Elektronen-Synchrotron DESY. The TESLA (TeV-Energy Superconducting Linear Accelerator) collaboration consists of 44 institutes from 10 countries and aims at the construction of a 500 GeV (center-of-mass) e^+/e^- linear collider with an integrated X-ray laser facility [11]. Major hardware contributions to TTF have come from Germany, France, Italy, and the USA. The present TTF layout (phase 1) is shown in Figure 3. The main parameters for FEL operation are given in Table I. In a second phase, the installation will be upgraded to a soft X-ray user facility [17, 18].

The injector is based on a laser-driven photocathode installed in a $1\frac{1}{2}$-cell radio-frequency (rf) cavity operating at 1.3 GHz [20] with a peak accelerating electric field of 37 MV/m on the photocathode. At the exit of the cavity the electron energy is 4 MeV. The Cs_2Te cathode [21] is illuminated by a train of UV laser pulses generated in a mode-locked solid-state laser system [22] synchronized

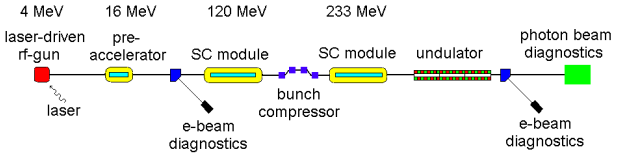

FIG. 3: Schematic layout of phase 1 of the SASE FEL at the TESLA Test Facility at DESY, Hamburg. The linac contains two 12.2 m long cryogenic modules each equipped with eight 9-cell superconducting (SC) accelerating cavities [19]. The total length is 100 m.

with the rf. It generates bunch charges of several nC at up to 2.25 MHz repetition rate [23]. The UV pulse length measured with a streak camera is $\sigma_t = 7.1 \pm 0.6$ ps . Experiments so far have operated with up to 70 electron bunches per second.

The gun section is followed by a 9-cell superconducting cavity, boosting the energy to 16 MeV. Two 12.2 m long accelerating modules each containing eight 9-cell superconducting niobium cavities [19] provide a beam energy of up to 300 MeV. In the first module the electrons are accelerated on the slope of the rf wave to impress a position-dependent energy distribution within the bunch, the front electrons receiving lower energy gain than the tail electrons. In the following magnetic chicane [24] the front particles move on a longer trajectory than the tail particles. Thereby the bunch lengths can be reduced by a factor of five. The second module accelerates the compressed bunches on the crest of the rf wave. The bunch compression is essential for obtaining the large peak currents that are needed in the SASE FEL.

Beam dynamics simulations indicate a peak current of $1-1.5$ kA within a short leading spike, followed by a long tail with much less current. The length of the spike can be tuned down to about 100 fs duration. Only this spike provides sufficiently high peak current to reach large FEL gain, and even saturation, within the available undulator length. As a consequence, the FEL radiation pulse length can be tuned by changing the length of this spike. The measurement of the FEL radiation pulse length (see below) is consistent with simulations of electron beam dynamics and of the FEL process.

The undulator is a permanent magnet device [25] with a 12 mm gap and an undulator parameter of K=1.17. Permanent-magnet quadrupole fields are superimposed on the periodic undulator field in order to focus the electron beam along the undulator. The undulator system is subdivided into three segments, each 4.5 m long and containing 10 quadrupole sections with alternating gradients. The total length of the system is 14.1 m. The vacuum chamber incorporates 10 beam position monitors and 10 dipole magnets per segment for orbit steering, one for each quadrupole magnet [26, 27]. For optimum overlap between the electron bunch and the emitted radiation, high precision on the magnetic fields and on the

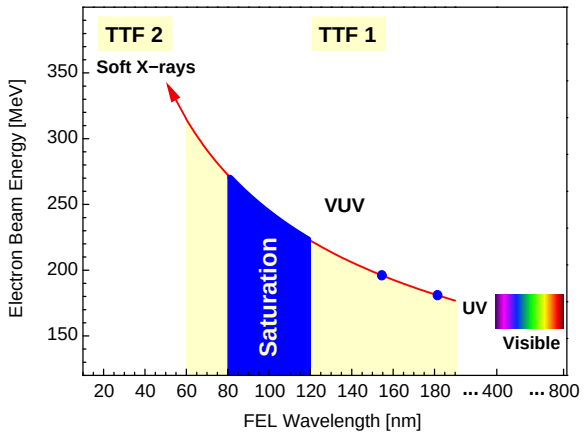

FIG. 4: VUV wavelength range within which lasing has been obtained at the TTF FEL, phase 1 (TTF1). The wavelength was tuned by changing the electron beam energy (vertical axis, cf. Eq. 1). The individual dots outside the range in which saturation has been achieved represent an FEL gain of typically > 1000 demonstrated in an earlier stage of the experiment [30]. After a linac upgrade to electron beam energies of up to 1 GeV (TTF 2), the FEL will enter the soft X-ray region [18].

TABLE I: Main parameters of the TESLA Test Facility for FEL experiments (TTF FEL, phase 1)

Electrons:	
beam energy	$220 - 270$ MeV
bunch charge	2.7-3.3 nC
charge in lasing part of bunch	0.1-0.3 nC
peak current	1.3 ± 0.3 kA
rms energy spread	150 ± 50 keV
rms normalized emittance	$(6 \pm 2)\pi$ mm·mrad
bunch spacing	0.44 / 1 μs
number of bunches in a train	up to 70
rf pulse repetition rate	1 Hz
Undulator:	
undulator period λ_u	27.3 mm
undulator peak field	0.47 T
average beta-function	1.2 m
magnetic length of undulator	13.5 m
Photons:	
radiation wavelength	80-120 nm
energy in the radiation pulse	$30 - 100$ μJ
FWHM radiation pulse duration	$50 - 200$ fs
radiation peak power level	1 GW
average radiation power up to	5 mW
spectral width (FWHM)	1%
rad. spot size at undulator exit (FWHM)	250 μm
radiation angular divergence (FWHM)	260 μrad

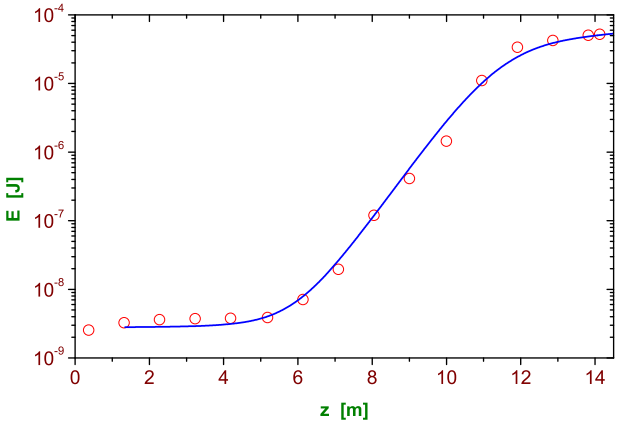

FIG. 5: Average energy in the radiation pulse as a function of the active undulator length. Circles: experimental results. Solid curve: numerical simulations with the code FAST [32], using parameters of Table 1.

mechanical alignment are required. The undulator field quality was adjusted such that the expected rms deviations of the electrons from the ideal orbit should be smaller than 10 μm at 300 MeV [28]. The beam orbit straightness in the undulator is determined by the alignment precision of the quadrupole magnets which is better than 50 μm in both vertical and horizontal direction.

EXPERIMENTAL RESULTS

Since the first lasing observed at the TTF [29] the performance of the SASE FEL has been steadily improved. By varying the energy of the linear accelerator, full wavelength tunability in a wide range from 80 to 180 nm [30] has been demonstrated, as depicted in Figure 4. Further work has been focused on the range from 80 nm to 120 nm by request of first scientific users. Recently, saturation has been achieved in this entire wavelength range.

For a characterization of the FEL process, the energy of the radiation as well as its spectral characteristics and angular distribution have been measured. Figure 5 presents the measured average energy in the radiation pulse as a function of the active undulator length, defined as the distance over which the electron beam and the photon beam overlap. The wavelength for this measurement was chosen at 98 nm. The active length of the undulator can be varied over a large range by generating suitable orbit displacements of the electron beam, making use of the steering dipole magnets mounted inside the undulator. The orbit deflection produced by a steerer is sufficient to inhibit the FEL amplification process downstream of this magnet. The radiation energy has been measured within a 10 mm aperture located 12 m behind the undulator. Two detectors have been used: A gold wire mesh scattering light onto a microchannel-plate detector [31] and a thermopile [33]. Both agree within 50% in the measured

pulse energy. When the electron and photon beam have insufficient overlap along the whole undulator, the FEL amplification is suppressed and the detector shows the expected level of spontaneous emission of about 2.5 nJ from the entire electron bunch, collected from the full undulator length. By providing a good overlap of the two beams over an increasing length of the undulator, the FEL amplification is gradually switched on and the radiation energy rises exponentially until a plateau is reached at a level of 30 to 100 μJ, depending on the accelerator tuning.

Figure 5 clearly exhibits the exponential growth of SASE power with the undulator length, yielding a power gain length of $L_g = 67 \pm 5$ cm. The almost constant level of radiation energy observed for an active undulator length of less than 5 m does not imply that there is no FEL gain in this part of the undulator. In contrast, this is due to the fact that in the first few meters of the undulator, the FEL radiation stays below the energy of spontaneous radiation accumulated over the entire undulator. In fact, extrapolation of the exponential gain curve down to the beginning of the undulator results in a pulse energy $P_0 \cdot A \cdot \tau_{\rm rad} \approx 0.3$ pJ (see Eq. 2; for determination of the duration of the radiation pulse $\tau_{\rm rad}$ see below), in good agreement with the equivalent input power P_0 of the shot noise from spontaneous radiation, estimated for a random electron distribution [6]. The important conclusion is that the entire undulator contributes to the SASE process, i.e. there are neither sections with too large undulator field errors nor local electron orbit distortions leading to imperfect overlap between electron and photon beam. We conclude that the FEL gain is about 10^7 in terms of effective power of shot noise. The measured power growth is also in agreement with the theoretical expectation. The solid curve in Figure 5 represents a three-dimensional numerical SASE simulation [34] using the electron beam and undulator parameters of Table I which were experimentally verified.

Measurements of the spectral distribution are presented in Figure 6. Single-shot spectra were taken with a monochromator of 0.2 nm resolution equipped with an intensified CCD camera [33] . The curve in the upper right corner represents the spectrum averaged over 100 bunches. The single shot spectra show an ensemble of a few peaks which reflect the number of longitudinal modes in the radiation pulse [35], as it is expected for SASE FEL radiation starting from shot noise.

The pulse duration is a very important parameter but presently not accessible to direct measurement in the time domain. The FWHM spectral width $\Delta\omega$ of each peak in the single shot spectrum is related to the approximate radiation pulse length by $\tau_{\rm rad} \simeq 2\pi/\Delta\omega$. For the spectra shown in Figure 6 this results in $\tau_{\rm rad} \simeq 50$ fs. To meet the requirements of scientific users, it is very important to tune the length of the radiation pulse in a well defined way. This can be done by varying the

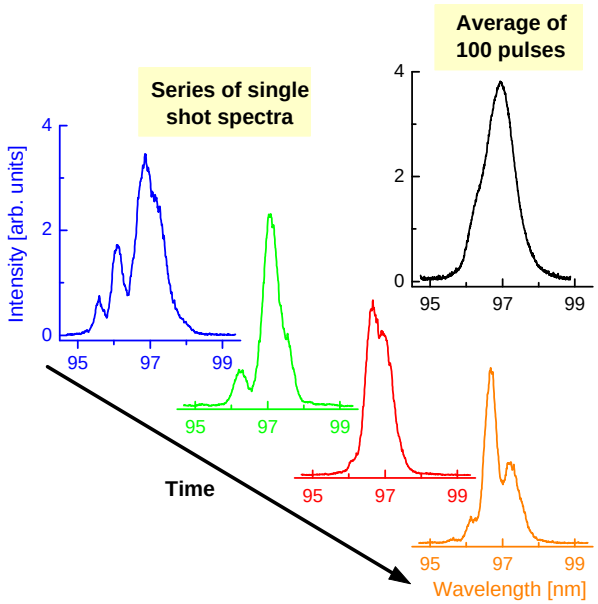

FIG. 6: Measured spectral distribution of the FEL radiation. Each single shot spectrum (originating from individual electron bunches) exhibits an ensemble of a few peaks corresponding to the fluctuation of the number of longitudinal modes of FEL radiation. This feature is characteristic for SASE FELs driven by shot noise. Since the center frequencies of these spikes are random (within the bandwidth of the FEL), they are smeared out in the averaged spectrum shown in the upper right corner.

bunch compressor settings, thus changing the length of the high-current spike in the electron bunch. Figure 7 compares single shot spectra for two bunch compressor settings. With a longer spike reaching high FEL gain, one expects more longitudinal modes in the radiation pulse and consequently more peaks within its spectral distribution, each peak having a correspondingly smaller width $\Delta\omega$. This is in accordance with our observation. For the long pulse setting illustrated in Figure 7 the estimated FWHM pulse duration is $\tau_{\rm rad} \simeq 2\pi/\Delta\omega \simeq 100$ fs. According to the theory of SASE FELs, the number of longitudinal modes M should be determined by both $\Delta\omega$ and the FWHM width $\Delta\omega_{\rm avg}$ of the averaged spectrum through $M = \sqrt{\pi}\Delta\omega_{\rm avg}/\Delta\omega$ [6], in reasonable agreement with spectra shown in Figures 6 and 7.

A more detailed understanding of the statistical and time domain properties can be achieved through an analysis of fluctuation measurements. These fluctuations have two different aspects which are intimately related to each other: Fluctuations of the single pulse spectra, illustrated in Figure 6, and fluctuations of the pulse-to-pulse intensity as shown in Figure 8 for the two different pulse length settings used for Figure 7.

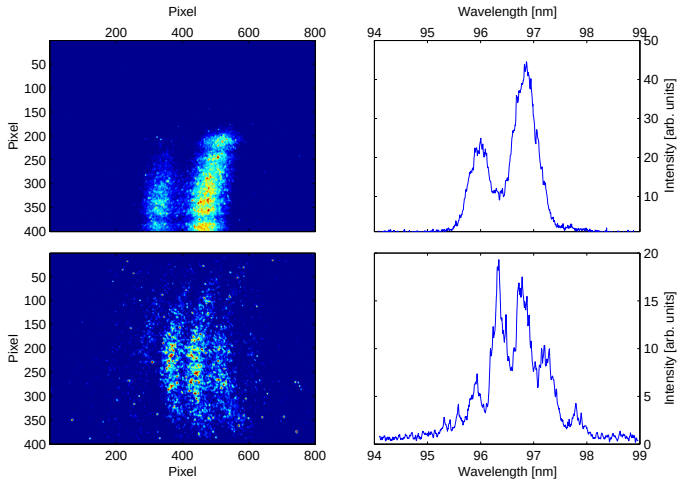

FIG. 7: Spectra from short (top) and long (bottom) FEL pulses. On the left hand side, the CCD image of the dispersed FEL radiation in the exit plane of the monochromator is shown in a false color code. The dispersive direction is in the horizontal. On the right hand side, the spectra are evaluated quantitatively along the horizontal center line of the CCD image. It is seen that the number of optical modes are different: For our short pulse setting (top) there are, in average, 2.6 modes, in the long pulse setting (bottom) there are 6 modes in average.

It is essential to realize that the fluctuations seen in Figure 8 are not due to unstable operation of the accelerator but are inherent to the SASE process. Shot noise in the electron beam causes fluctuations of the beam density, which are random in time and space [36]. As a result, the radiation produced by such a beam has random amplitudes and phases in time and space and can be described in terms of statistical optics. In the regime of exponential growth, the radiation pulse energy is expected to fluctuate according to a gamma distribution $p(E)$ [35],

$$p(E) = \frac{M^M}{\Gamma(M)} \left(\frac{E}{\langle E\rangle}\right)^{M-1} \frac{1}{\langle E\rangle} \exp\left(-M\frac{E}{\langle E\rangle}\right) \qquad (3)$$

where $\langle E\rangle$ is the mean energy, $\Gamma(M)$ is the gamma function with argument M, and $M^{-1} = \langle(E-\langle E\rangle)^2\rangle/\langle E\rangle^2$ is the normalized variance of E. The parameter M corresponds to the number of optical modes, which is in fact identical to the number of longitudinal modes introduced before, because the radiation is transversely coherent (see below). As can be seen from Figure 8 the observed distribution of the energy in the radiation pulses is in good agreement with the gamma distribution for both pulse length settings. The relative rms fluctuations are about 61% and 41%, respectively. The values for M extracted from fluctuation analysis, agree with those achieved from single shot spectral analysis qualitatively.

A special case is $M = 1$, which can be realized by applying a narrow monochromator window to the FEL radiation, for instance to the spectra displayed in Figure 6. We have used a spherical grating in Littrow mounting with a resolution of about $\Delta\omega/\omega \simeq 10^{-4}$ [37]. In this case, Eq. 3 predicts a negative exponential distribution in agreement with the data in Figure 8. Note that the same kind of statistics applies for completely chaotic polarized light, in particular for spontaneous undulator radiation. In the end, it is the good agreement of fluctuation analysis with the model of chaotic polarized light which justifies the extraction of the pulse duration from single shot spectra as done here.

The energy distribution differs from a gamma distribution when the laser saturation level is reached. It is worth noting that the observed distribution (Figure 9) is also well reproduced by the numerical simulation without having to introduce any new parameters beyond those needed in the exponential regime.

A crucial feature is the transverse coherence of the FEL radiation [38]. Figure 10 shows two diffraction patterns of the FEL radiation measured in a distance of 3 m behind a double slit and two crossed slits (see pictographs), respectively. The images displayed in the upper part of the figure have been recorded with a gated CCD camera viewing a Ce:YAG fluorescent screen, which converts the VUV radiation to visible light. The intensity profiles in the lower part represent horizontal cuts through the centre of the corresponding diffraction pattern. The remarkably high fringe visibility is a proof of the high degree of transverse coherence. The less pronounced minima in the left part of the double slit profile may be explained by the varying focusing properties of the CCD camera due to the observation angle of 45° or by inhomogenities of the yield of the Ce:YAG crystal. The transverse coherence of the FEL radiation illustrated by the diffraction patterns has been corroborated by measurements of the opening angle of the radiation [34].

With a number of $2 \cdot 10^{13}$ photons per pulse, a pulse length of 50 fs and the full transverse coherence, the peak brilliance is $2 \cdot 10^{28}$ photons/(s $\cdot$ mrad^2 $\cdot$ mm^2 $\cdot$ (0.1% bandwidth)), eight orders of magnitude higher than at third generation synchrotron radiation sources (cf. Figure 2), and the peak radiation power is about a gigawatt. The degeneracy parameter (the number of photons per mode) is about 10^{13} and thus in the same order of magnitude as for quantum lasers operating in the visible light regime and more than two orders of magnitude above values achieved by High Harmonic Generation (HHG) from conventional laser light into the VUV [13].

CONCLUSION AND OUTLOOK

A new generation of radiation sources for VUV radiation at wavelengths in the 100 nm range has become

available exceeding the peak brilliance of other existing sources by several orders of magnitude. Due to the basic underlying principle, full wavelength tunability and adjustable pulse lengths below 100 fs are possible and have been demonstrated.

The device will be upgraded to a user facility for soft X-rays available for scientific users starting in 2004. The demonstrated technology is also suitable to realize a X-ray laser user facility for Ångström wavelengths [9–11], such as proposed within the TESLA project.

[1] J.M.J. Madey J. Appl. Phys. **42**, 1906 (1971).
[2] D.A.G. Deacon et al., Phys. Rev. Lett. **38,** 892 (1977).
[3] W.B. Colson Nucl. Instr. and Meth. **A475,** 397 (2000).
[4] K.J. Kim, Phys. Rev. Lett. **57,** 1871 (1986).
[5] S. Krinsky, L.H. Yu, Phys. Rev. **A35,** 3406 (1987).
[6] E.L. Saldin, E.A. Schneidmiller, M.V. Yurkov, "The Physics of Free Electron Lasers", Springer (1999) and references therein.
[7] A.M. Kondratenko, E.L. Saldin, Part. Accelerators **10,** 207 (1980).
[8] R. Bonifacio, C. Pellegrini, L.M. Narducci, Opt. Commun. **50,** 373 (1984).
[9] H. Winick et al., Proc. PAC Washington and SLAC-PUB-6185, (1993).
[10] R. Brinkmann et al., Nucl. Instr. and Meth. **A 393,** 86-92 (1997).
[11] F. Richard et al. (eds.),TESLA Technical Design Report, DESY2001-011, and http://tesla.desy.de.
[12] H.-D. Nuhn, J. Rossbach, Synchrotron Radiation News **13**, No. 1, 18 - 32 (2000).
[13] E. Constant et al., Phys. Rev. Lett. **82,** 1668 (1999).
[14] M. Hogan et al., Phys. Rev. Lett. **81,** 4867 (1998).
[15] S. Milton et al., Science **292,** Iss. 5524, 2037 (2001).
[16] W. Brefeld et al., Nucl. Instr. and Meth. **A393,** 119-124 (1997).
[17] T. Åberg, et al., A VUV FEL at the TESLA Test Facility at DESY, Conceptual Design Report, DESY Print TESLA-FEL 95-03 (1995).
[18] J. Rossbach Nucl. Instr. and Meth. **A 375,** 269 (1996).
[19] H. Weise, Proc. 1998 Linac Conf. Chicago, 674-678 (1998).
[20] J.-P. Carneiro, et al., Proc. 1999 Part. Acc. Conf., New York, 2027-2029 (1999).
[21] D. Sertore et al., Nucl. Instr. and Meth. **A445,** 422 (2000).
[22] I. Will, S. Schreiber, A. Liero, W. Sandner, Proc. 1999 FEL Conf, Hamburg, II-99, Elsevier (2000).
[23] S. Schreiber, I. Will, D. Sertore, A. Liero, W. Sandner, Nucl. Instr. and Meth. **A445,** 427 (2000).
[24] T. Limberg et al., Nucl. Instr. and Meth. **A375,** 322 (1996).
[25] Y. M. Nikitina, J. Pflüger, Nucl. Instr. and Meth. **A375,** 325 (1996).
[26] U. Hahn, J. Pflüger, G. Schmidt, Nucl. Instr. and Meth. **A429,** 276 (1999).
[27] U. Hahn et al., Nucl. Instr. and Meth. **A445,** 442 (2000).
[28] J. Pflüger, Nucl. Instr. and Meth. **A445,** 366 (2000).
[29] J. Andruszkow et al., Phys. Rev. Lett. **85** 3825 (2000).
[30] J. Rossbach et al., Nucl. Instr. and Meth. **A475,** 13 (2001)
[31] B. Faatz et al., DESY Print TESLA-FEL 2001-09 (Contributions to the FEL2001 Conference, August 20-24, 2001, Darmstadt, Germany), pp. 62-67.
[32] E.L. Saldin, E.A. Schneidmiller, M.V. Yurkov, Nucl. Instr. and Meth. **A429**, 233 (1999).
[33] R. Treusch et al., Nucl. Instr. and Meth. **A445**, 456 (2000).
[34] V. Ayvazyan et al., Phys. Rev. Lett.**88,** No.10 (2002).
[35] E.L. Saldin, E.A. Schneidmiller, M.V. Yurkov, Opt. Commun. **148**, 383 (1998).
[36] R. Bonifacio, et al., Phys. Rev. Lett. **73,** 70 (1994)
[37] B. Faatz et al., Nucl. Instr. and Meth. **A429**, 424 (1999).
[38] L. Kipp et al., Nature **414**, 184 (2001)

ACKNOWLEDGEMENTS

The authors are grateful for the invaluable support by the technical staff of the participating groups in the TESLA collaboration [11].

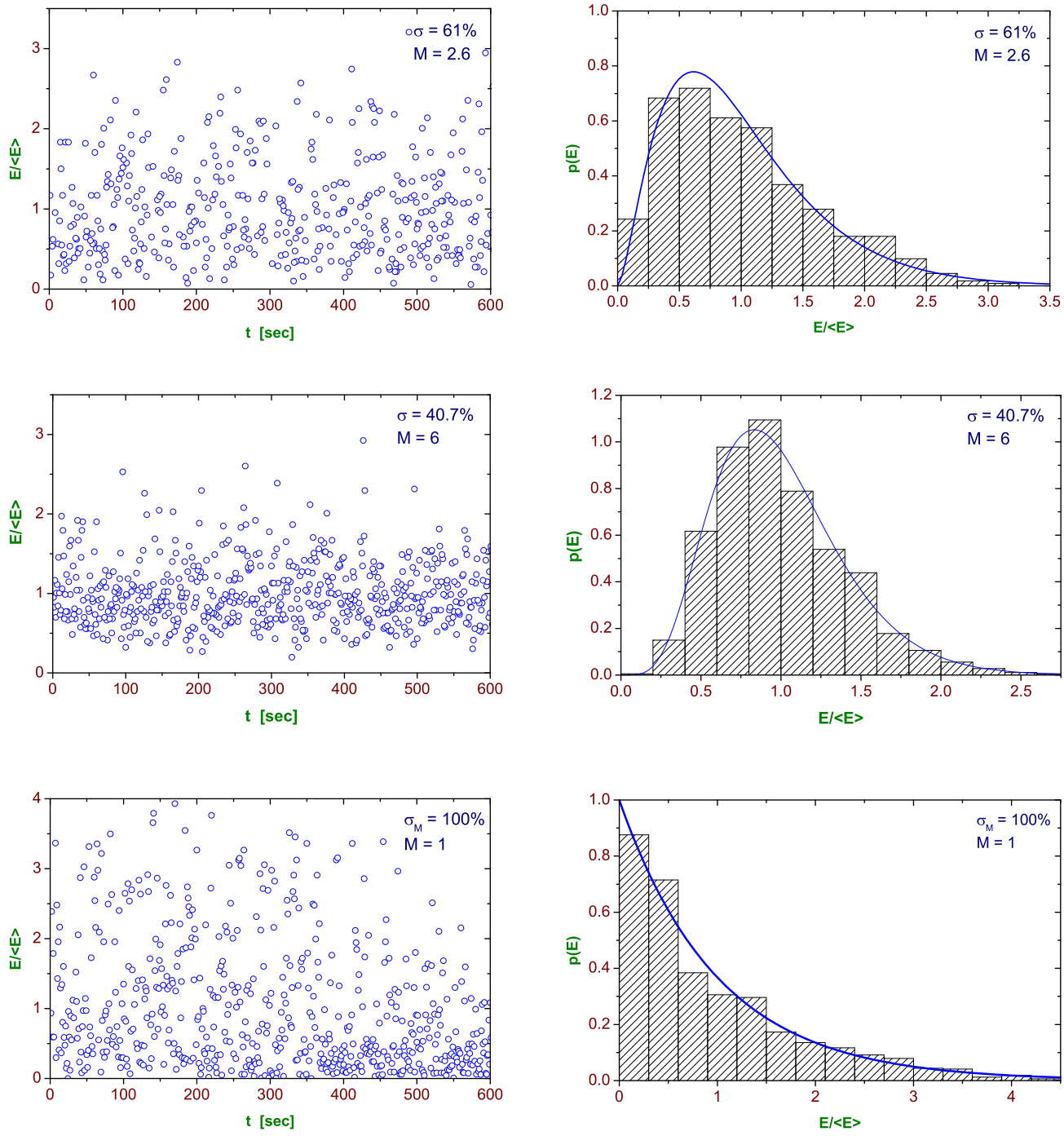

FIG. 8: Pulse-to-pulse fluctuation of SASE pulse energy for different settings of electron bunch length. Left column: measured single pulse energy versus time; Right column: histogram of probability distribution extracted from the measurement. The SASE pulses are observed at high gain, but still in the exponential regime, not yet in laser saturation, cf. Figure 5. The upper plot is for short electron bunch setting (equal to the setting used for Figure 7, top), the middle plot is for long electron bunch setting (equal to the setting used for Figure 7, bottom), and the lower one is for the radiation pulse having passed a narrow-band monochromator. The solid curves represent gamma distributions according to Eq. 3 with the mode number $M = \sigma^{-2}$ calculated from the standard deviation σ of each distribution.

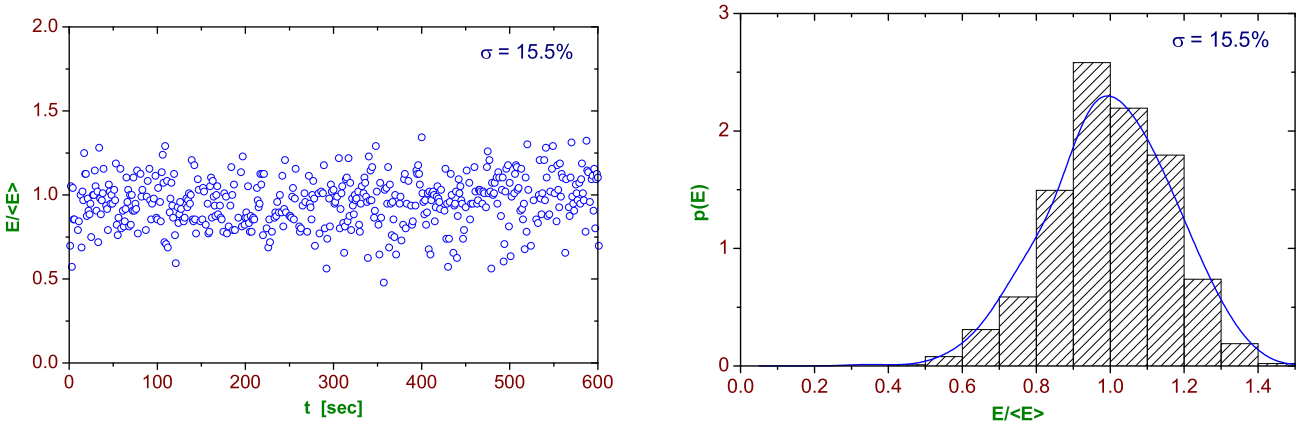

FIG. 9: Pulse-to-pulse fluctuation of SASE pulse energy in saturation regime. The electron beam was in short bunch setting, cf. the upper plots in Figure 8. The solid line represents a numerical simulation with the code FAST [32].

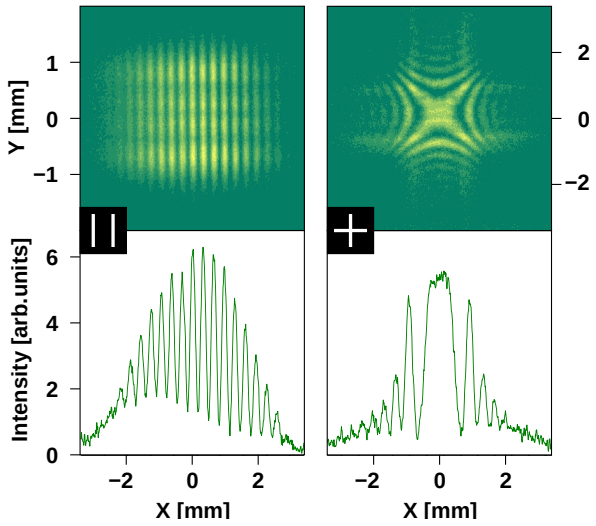

FIG. 10: Diffraction patterns of two different slit arrangements (see pictographs) illustrating the transverse coherence of the FEL radiation.
left: double slit, each slit 2 mm (vert) × 200μm (horiz.), horizontal slit separation 1 mm
right: crossed slits, each slit 4 mm× 100μm
The slits are located 12 m behind the exit of the undulator. The images have been recorded with a gated CCD camera viewing a Ce:YAG fluorescent screen 3 m behind the slits. They have been taken as a sum of a few consecutive FEL pulses with a wavelength of 95 nm. The lower part of both images depicts a horizontal cut through the centre of the respective diffraction pattern.